Honeywell Report 12013-QR 2

12 November 1965

PROGRESS REPORT

DESIGN OF A

LOAD RELIEF CONTROL SYSTEM

National Aeronautics and Space Administration
George C. Marshall Space Flight Center
Contract NAS8-20155

Contributors:

G. B. Skelton
C. R. Stone
E.R.R.

Approved by: O. Hugo Schuck
O. Hugo Schuck
Director of Research

Honeywell, Inc.
Systems and Research Division
Research Department
2345 Walnut Street
St. Paul, Minnesota

4626

12013-QR 2 November 12, 1965

DESIGN OF A LOAD RELIEF CONTROL SYSTEM

ABSTRACT

This is the second quarterly progress report submitted in accordance with the provisions of Contract NAS8-20155. It contains a review of the current project status, discussion of the computational results obtained to date, and discussion of the generation of wind-induced missile bending-moments. The analysis requirements of the study are almost completed, and the "direct-iteration" routine is considered powerful and sufficient for determining optimum control gains. It is suggested that future work be based on a more realistic bending-moment-rate expression.

TABLE OF CONTENTS

Appendices

SECTION I

PROJECT STATUS

This section contains brief descriptions of the current technical status of the project, work accomplished in the reporting period, preliminary conclusions, and anticipated work. Details are presented in the Technical Discussion, Section III.

For convenience, reference to previous progress reports, Honeywell Reports 12013-PR 1, 2, 3, 4 and 12013-QR 1, will be indicated by the notations (PR1), (PR2), (QR1), etc.

A. Current Status

This subsection contains brief descriptions of the current status of the project milestones listed in the accompanying program chart.

TASK 1. Preparation

1a. Develop Wind Model. Status: Complete. The derivation of the model was presented in (QR 1) and the calculated model coefficients in (PR 3).

1b. Write Equations of Motion. Status: Complete. Equation forms and coefficient values were presented in (QR 1). Anomalies discovered in the bending-moment-rate expression were reported in (QR 1) and (PR 3). The results of our investigation of these anomalies are presented in Appendix A of this report.

1c. Program Equations. Status: Complete. The programmed equations include an arbitrarily modified bending-moment-rate expression.

1d. Present Results of Computations. Status: Complete. Uncontrolled vehicle mean-wind responses were presented in (PR3). Uncontrolled vehicle response covariances are presented in Appendix B of this report.

TASK 2. Analysis

2a. Algorithm for g_1 and g_2. Status: Complete. The derivation of the algorithms was presented in (PR1) and (PR3). It was shown in (PR3) that the optimum solution would not produce infinite gains and zero covariances.

2b. Program algorithm. Status: Partially complete. The direct iteration algorithm presented in (PR3) has been programmed.

2c. Compute. Status: Partially complete. Results obtained with the direct iteration algorithm are presented in Appendix C of this report. The arbitrarily modified bending-moment-rate expression was employed in obtaining these results.

TASK 3. Simulation. Status: Partially complete. The response covariances of the minimax controller developed under Contract NAS8-11206 (reported in Honeywell Report 12003-PR 15) have been calculated and are presented in Appendix D of this report.

TASK 4. Reporting. Status: Four monthly progress reports and one quarterly progress report have been submitted.

B. Preliminary Conclusions

All analyses to date have employed the arbitrarily modified bending-moment-rate expression. It now appears that the direct-iteration routine described in (PR3) is sufficient for determining a satisfactory controller, and the gradient routine described in (PR1) need not be employed.

C. Progress During Reporting Period

All of the results presented in Appendices B, C, D were obtained during the reporting period.

The theoretical analyses reported in Appendix A were obtained in the previous reporting period, but illness in Mr. Stone's family precluded their presentation in the previous report (PR4). The coefficient values presented in Appendix A were obtained in the current reporting period.

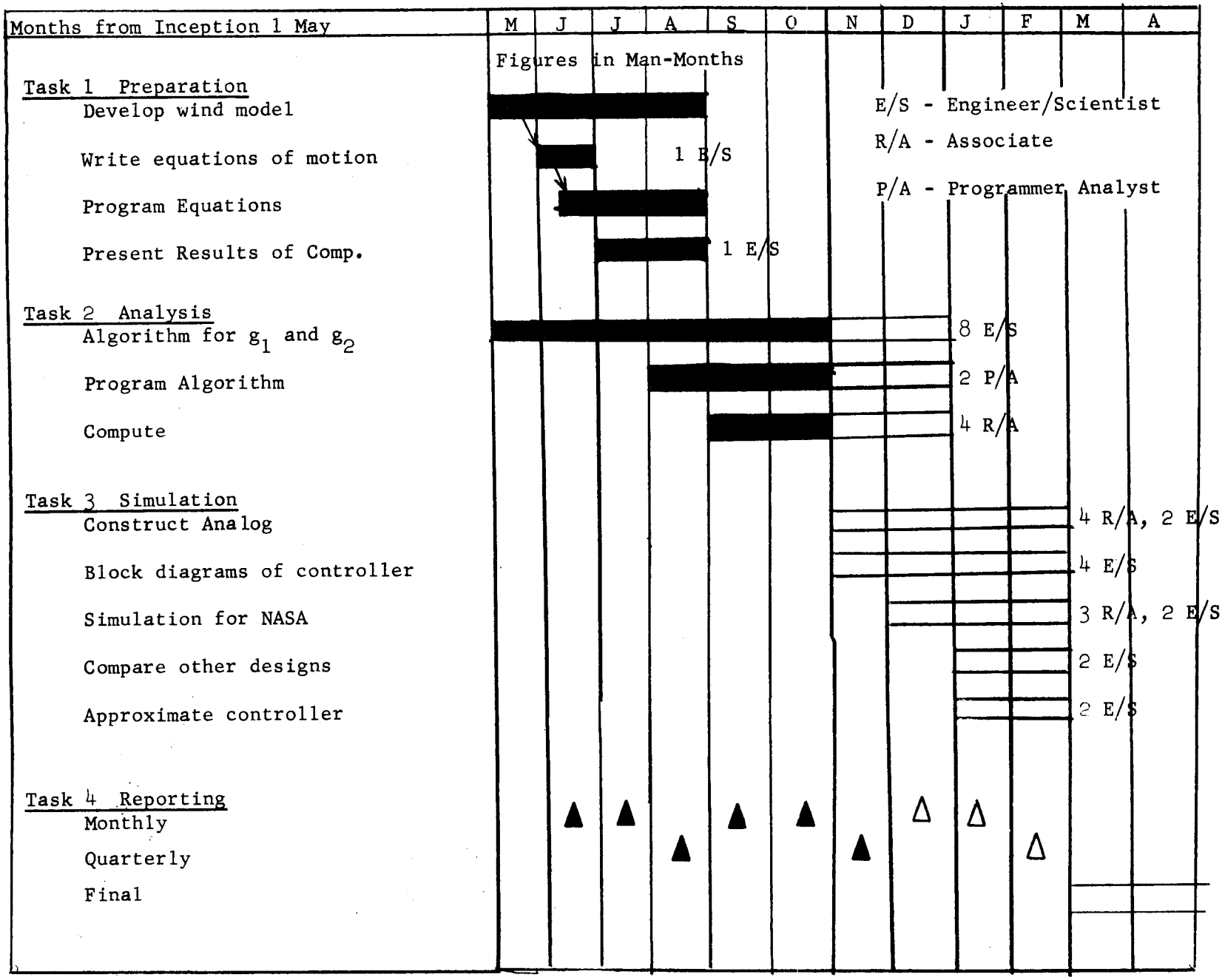
Months from Inception 1 May
M J J A S O N D J F M A
Figures in Man-Months
E/S - Engineer/Scientist
R/A - Associate
P/A - Programmer Analyst
Task 1 Preparation
Develop wind model
Write equations of motion
1 E/S
Program Equations
Present Results of Comp.
1 E/S
Task 2 Analysis
Algorithm for g_1 and g_2
8 E/S
Program Algorithm
2 P/A
Compute
4 R/A
Task 3 Simulation
Construct Analog
4 R/A, 2 E/S
Block diagrams of controller
4 E/S
Simulation for NASA
3 R/A, 2 E/S
Compare other designs
2 E/S
Approximate controller
2 E/S
Task 4 Reporting
Monthly
Quarterly
Final

D. Anticipated Work.

1. Analysis. The bending-moment-rate expression described in Appendix A of this report is in a distributed parameter form (an integral over vehicle length), and it is computationally inconvenient to employ it as stated. We shall attempt to derive a suitable lumped-parameter expression.

Given such an expression, the minimizing control gains will be recalculated with the direct iteration routine. The effects of varying the gimbal-angle limit, the bending moment limit, etc., will then be examined.

An attempt will be made to determine the causes of gain-peaks, sign changes, etc. Controller variations are produced by variations of the vehicle equation coefficients and by the form of the cost expression, but few of the causal relations have been identified.

2. Simulation. The analog simulation and comparison studies (Task 2 above) will be started. Gains obtained with the arbitrarily modified bending-moment-rate expression will be employed until gains computed with a more accurate expression become available.

SECTION III

TECHNICAL DISCUSSION

Four topics are discussed in this section. The arbitrarily modified bending-moment-rate expression employed to date is first presented. Significant computational details of the direct-iteration routine are next presented. The results presented in Appendices B, C, D are then discussed. The section concludes with discussion of the present project status and anticipated future work.

A. Bending Moment Rate.

The "Model Vehicle #2" bending-moment expression is

$$I_b = M'_\beta \beta + M'_\alpha \alpha$$
$$= M'_\beta \beta + M'_\alpha \left[-\frac{\dot{z}}{v} + \varphi + \frac{v_\omega}{v}\right],$$

where

I_b = bending moment

β = gimbal angle

$\dot{z}$ = drift rate

φ = attitude

v_ω = side wind velocity

v = vehicle velocity.

Direct differentiation of this equation yields

$$\dot{I}_b = \dot{M}'_\beta \beta + M'_\beta \dot{\beta} + \dot{M}'_\alpha \left[-\frac{\dot{z}}{v} + \varphi + \frac{v_\omega}{v}\right]$$
$$+ M'_\alpha \left[-\frac{\ddot{z}}{v} + \frac{\dot{z}}{v^2}\dot{v} + \dot{\varphi} + \frac{\dot{v}_\omega}{v} - \frac{v_\omega}{v^2}\dot{v}\right].$$

Substitution of the vehicle model and wind model equations from (QR1) produces the bending-moment-rate

$$\dot{I}_b = M'_\alpha \ddot{\varphi} + \frac{M'_\alpha}{v} H\dot{h}x + \left[-\frac{\dot{M}'_\alpha}{v} + \frac{M'_\alpha}{v^2}\dot{v} + \frac{M'_\alpha}{v}\frac{N'}{Mv}\right]\dot{z}$$

$$+ \left[\dot{M}'_\beta - \frac{M'_\alpha}{v}\frac{R}{M} - 14.6M'_\beta\right]\beta + \left[\dot{M}'_\alpha - \frac{M'_\alpha}{v}\left(\frac{F-X}{M} + \frac{N'}{M}\right)\right]\varphi$$

$$+ \left[\frac{\dot{M}'_\alpha}{v}H + \frac{M'_\alpha}{v}\dot{H} - \frac{M'_\alpha}{v}H\dot{v} - \frac{M'_\alpha}{v}\frac{N'}{Mv}H\right]\omega + 14.6\,M'_\beta u$$

$$+ \left[\frac{\dot{M}'_\alpha}{v} - \frac{M'_\alpha}{v^2}\dot{v} - \frac{M'_\alpha}{v}\frac{N'}{Mv}\right]\bar{v} + \frac{M'_\alpha}{v}\dot{\bar{v}}_\omega + d_2\sqrt{h}\,\frac{M'_\alpha H}{v}\,\eta\,,$$

where

h = altitude

$\bar{v}_\omega$ = mean wind

H_ω = wind deviation from mean

x = second wind state

η = white noise input to wind filter.

This expression was objected to in (QR1) because it contained η, the white noise input to the wind filter. It was objected to in (PR3) because of the extreme time-variations of the $\dot{z}$, $\bar{v}_\omega$, and ω coefficients. The variations were large enough to prevent approximating the wind and vehicle differential equations with 1/100 sec. difference equations. The $\dot{z}$, $\bar{v}_\omega$, ω, and η terms all appear to be physically unrealistic.

These observations prompted the study of the bending-moment equation presented in Appendix A of this report.

The above equation was modified and used in the analyses to provide a mathematical vehicle for testing the direct-iteration routine. The η white noise term was dropped from the equation, and the $\dot{z}$, $\bar{v}_\omega$, and ω coefficients were arbitrarily

smoothed. The original coefficients and the modified coefficients employed in the analyses are presented in Appendix E of this report. No claim of realism is made for the resulting bending-moment-rate expression.

B. Computational Details.

Several of the computational details of the direct iteration routine are noted so that other investigators of similar problems can avoid pitfalls we encountered.

1. It is difficult to compute the sum

$$1 - \int_{-\infty}^{\alpha} \frac{1}{\sqrt{2\pi}} e^{-\frac{x^2}{2}} dx$$

for large values of $\alpha(\alpha \geq 4)$ due to computer round-off errors. The approximation

$$1 - \int_{-\infty}^{\alpha} \frac{1}{\sqrt{2\pi}} e^{-\frac{x^2}{2}} dx \simeq \frac{1}{\sqrt{2\pi}} \frac{e}{\alpha}^{-\frac{\alpha^2}{2}}$$

was employed in our analyses. The accuracy of the approximation increases with increasing α and it is correct to two significant digits at $\alpha = 0$.

2. For small values of α $(\alpha \leq 4)$ the Gaussian integral can be obtained to as many digits as the computer is capable of carrying by truncating the power series

$$\int_0^{\alpha} \frac{1}{\sqrt{2\pi}} e^{-\frac{x^2}{2}} dx = \frac{1}{\sqrt{2\pi}} \int_0^{\alpha} \sum_{i=0}^{\infty} \frac{(-1)^i (x)^{2i}}{i! 2^i}$$

$$= \frac{1}{\sqrt{2\pi}} \sum_{i=0}^{\infty} \frac{(-1)^i (x)^{2i+1}}{i! 2^i (2i+1)}$$

after j terms with the ratio test

$$\frac{(x)^{2j+1}}{j!2^j(2j+1)} \Bigg/ \sum_{i=0}^{j} \frac{(-1)^i(x)^{2i+1}}{i!2^i(2i+1)} < 10^{-N},$$

where N is the number of significant digits desired. N = 9 was employed in our analyses.

3. On the Honeywell 1800 computer employed in our analyses, any exponential with an argument less than -128 is automatically set to zero. We were therefore forced to set the function $e^{-\frac{1}{2}\left(\frac{\gamma}{\sigma}\right)^2}$ to zero for $\gamma/\sigma > 16$. This automatically produced zero gimbal and bending-moment likelihood densities over a great portion of the flight time.

4. A 1/100 second sampling interval was chosen for approximating the vehicle model and wind model differential equations with difference equations. Computer storage limitations prevented storing model coefficient values at each 1/100 sec. instant over the 150 sec. flight. We decided to store the coefficient values at five second intervals and obtain the intermediate values by linear interpolation:

$$c(n\cdot\Delta t + M.5) = c(M.5) + \frac{n}{200}\,(C(M.5+5) - C(M\cdot 5)),$$

where $0 \leq n < 500$, $0 \leq M \leq 30$.

To avoid having to compute the products $\frac{n}{500}\,(C(M\cdot 5+5)-C(M\cdot 5))$ in each 1/100 sec. interval, we stored the initial values C(0), the final values C(150), and the increments $\frac{1}{500}\,(C(M\cdot 5+5) - C(M\cdot 5))$. This permitted updating or backdating coefficient values by adding or subtracting the stored increments, thereby avoiding the n/500 multiplication.

Computer round-off errors were encountered with this routine. The large (orders of magnitude) variations of some of the coefficients implied adding very small numbers to very large numbers, and we found that the final values produced by forward computation from the initial values differed from the original final values. These differences caused serious problems, as some always-positive coefficients which converged to zero at the final time were made to converge to negative final values. The sign reversals, of course, greatly affected the values of the control gains produced by the routines.

This problem was circumvented by truncating the original coefficient values to five significant digits. By doing this the coefficients and increments always could be added with no round-off errors.

C. Results of Analysis

The computation results presented graphically in Appendices B, C and D of this report are discussed in this subsection.

1. Uncontrolled Vehicle Responses.

The responses of the uncontrolled vehicle to the (NASA TN D-561, Patrick AFB, March) mean wind were presented in (PR3). The uncontrolled vehicle response covariances to the (QR1) second-order stochastic wind model are presented in Appendix D of this report.

The second graph, B2, of bending-moment-rate covariance employed the arbitrarily modified bending-moment-rate expression discussed in Section IIIA of this report.

The logarithmic scale of the ordinates should be noted.

The ratios of the response covariances to the squares of the amplitude limits imposed (QR1) indicate the need for vehicle control. The limits imposed were:

$|I_b| < 2.25*10^6$ Kilopons throughout the flight

$|\dot{\varphi} + .388\alpha| < 0.0453$ rad/sec at T = 150 sec.

$|z| < 3000$ meters at T = 150 sec.

$|\dot{z}| < 40$ meters/sec at T = 150 sec.

The graphs show that

$$\text{cov}\{I_b(t)I_b(t)\} < (2.25*10^6)^2 \quad \text{for } t < 55 \text{ sec}$$

$$\text{cov}\{(\dot{\varphi}(t) + .388\alpha(t))(\dot{\varphi}(t) + .388\alpha(t))\} < (0.0453)^2 \quad \text{for } t < 45 \text{ sec}$$

$$\text{cov}\{z(t)z(t)\} < (3000)^2 \quad \text{for } t < 65 \text{ sec}$$

$$\text{cov}\{\dot{z}(t)\dot{z}(t)\} < (40)^2 \quad \text{for } t < 45 \text{ sec.}$$

These numbers indicate that application of control during the early portions of the flight is probably not necessary.

2. Controller Determination

As discussed in (PR3), the direct-iteration technique is based on properly choosing the weights in a quadratic cost-form so that the controller minimizing the quadratic cost would also minimize the original sum-of-likelihoods cost. The quadratic weights are rechosen until the coefficients of the first variations of the quadratic and likelihoods costs are identical.

Two advantages for this technique were claimed. First, the gains minimizing the quadratic cost could be obtained without iteration by employing the results presented in (PR1). That is, first guesses would produce reasonable gains, reasonably near to the gains minimizing the sum-of-likelihoods cost. Secondly, the effects of varying quadratic weights on vehicle responses are intuitively much clearer than the effects of direct gain variations. Increasing the weight of a particular response would decrease the covariance of that response at the expense of other response covariances. This implies reasonable convergence times.

The direct-iteration technique has been programmed and run. After considerable program debugging, four runs of one iteration each were made with arbitrarily selected quadratic weights to provide a basis for selecting initial weights for iteration. Each iteration of the weights requires approximately fourty minutes computation time, the time being almost equally divided between gain computation and response covariance computation.

The results obtained from these initial passes were surprising. The response covariances produced were much lower than expected. During much of the flight the bending-moment and bending-moment-rate covariances are sufficiently low that the computed likelihood densities are lower than our ability to compute them, as discussed in Section IIIB above. The gimbal-angle likelihood densities were lower than could be computed throughout the flight. The final time likelihoods were also very low.

The results of the fourth of the initial iterations are presented in Appendix C of this report. These particular results are unsatisfactory in only one respect - the weight on the staging cost, $\dot{\varphi} + .388\alpha$, was too low, and the resulting final covariance of that term is too large. The various likelihoods produced by the system are

Probability that $|\beta(t)|$ exceeds 5 degrees at least once during the flight = (too low to compute)

Probability that $|I_b(t)|$ exceeds 2.25×10^6 kilopons at least once during the flight = 1.64×10^{-6}

Probability that $|\varphi + .388\alpha| > 0.0453$ rad/sec at the terminal time = 0.424

Probability that $|z| > 3000$ meters at the terminal time = (too low to compute)

Probability that $|\dot{z}| > 40$ meters at the terminal time = (too low to compute).

The feedback gains of the controller are presented in Figures C1.11 through C1.72, and the corresponding deterministic input in Figures C1.81 and C1.82.

It is noticed first that the gimbal angle feedback, Figure C1.4, is relatively constant over the flight time. The gimbal-actuator differential equation employed satisfied

$$\dot{\beta} = -14.6 + 14.6u\,.$$

The β-feedback varies between 0.6 and 0.997, and is approximately 0.9 during most of the flight. The 0.9 value produces

$$\dot{\beta} = -1.46\beta + 14.6(u - 0.9\beta)$$

and indicates a 10:1 decrease in the gimbal feedback. That is, the gimbal actuator has a lower break frequency than before.

The reason for this is the requirement for reduction of $\dot{\beta}$ implied by the cost form (PR1). Reducing $\dot{\beta}$ reduces the likelihood that β will exceed its amplitude limit.

All of the controller curves exhibit large variations during the final few seconds of flight. This is expected (large final-time variations have been observed in every quadratic-minimization, terminal-cost problem we have solved). It is due partly to the change of control emphasis from β and I_b to $\dot{\varphi} + .388\alpha$, z, and $\dot{z}$ towards the end of the flight. The major cause is the decrease in the need for damping in the final few seconds of flight.

Six of the gains (all but the β-gain and the deterministic input) change sign between 148 seconds and 149 seconds. Some are seen to peak during the high dynamic-pressure portion of the flight, while others change sign there. We have not had an opportunity to determine the causes of these various effects.

The vehicle mean-responses are presented in Figures C2.1 through C2.7. These are the responses to the mean wind and the deterministic input of Figures C1.81, C1.82. Two curves are presented on each graph, one where the controller was engaged at t = 0 sec. and the second where the controller was engaged at t = 40 sec.

The vehicle response covariances are presented in Figures C3.1 through C3.7. Again t = 0 sec and t = 40 sec. curves are shown. The significant aspects of these curves are the high bending moment covariances in the high dynamic-pressure region, the increase of bending, gimbal and staging covariances at the end of the flight, the relatively constant drift and drift-rate covariances, and the sharp decrease of the latter covariances at the end of the flight. The sharp final time variations of the covariances are an expected property of the solution - the weights on drift and drift rate were large, and the entire final control effort is directed towards reducing these two responses.

The t = 40 sec. responses are in general worse than the t = 0 sec. responses. This is expected, as earlier engagement of the controller produces smaller initial conditions at t = 40 sec.

The bending moment likelihood densities are presented in Figure C4 for the two engagement times. It is seen that the likelihood of exceeding the bending moment limit is essentially zero during the early portion of the flight and during most of the time after leaving the high dynamic pressures. The final time peaking up of the curves is produced by the control emphasis on reducing drift and drift-rate.

A property of a stationary random process is that displacements and time-rates of change of displacements are uncorrelated. If the controlled vehicle in this

problem behaved like a stationary process the correlation coefficients

$$\frac{|\mathrm{cov}\{\beta(t)\dot{\beta}(t)\}|}{\sigma_{\beta}(t)\ \sigma_{\dot{\beta}}(t)} \quad , \qquad \frac{|\mathrm{cov}\{I_b(t)\dot{I}_b(t)\}|}{\sigma_{I_b}(t)\ \sigma_{\dot{I}_b}(t)}$$

would be approximately zero. The implication of "almost" stationarity is that application of stationary (infinite time, conventional) control design procedures might be successful.

The above correlation coefficients are plotted versus time in Figure C5 for the t = 0 sec. controller-engagement case. It is evident that there is hope for infinite-time-control procedures during the intermediate flight times, but the system does not behave like a stationary process during the final portion of the flight. This is due to the character of the problem - infinite-time design procedures are not applicable in the final seconds of a finite-time control problem.

The results as a whole are most encouraging, and indicate that one can quickly design an excellent controller with quadratic minimization techniques.

D. Minimax Control

The response covariances of the minimax controller developed under Contract NAS8-11206 (reported in Honeywell Report 12003-PR 15) were obtained and are presented in Figures D1 through D7, Appendix D.

The minimax controller was developed only for the first eighty seconds of flight. The basis of the technique was to break the eighty seconds into short intervals over which the vehicle response equations could be approximated by constant coefficient equations. The technique then found the best linear controller of the form

$$\beta = k_1\varphi + k_2\dot{\varphi} + k_3\alpha$$

(actuator dynamics were ignored) for each interval, where the best controller would

minimize the maximum excursions of selected linear combinations of responses at the end of the interval. The only questionable aspect of this controller design procedure is that the initial conditions at the beginning of each constant coefficient interval were assumed zero - that is, final conditions of previous intervals were not carried forward.

The controller was tested with the gimbal actuator in place, so that the control input was

$$u = k_1\varphi + k_2\dot{\varphi} + k_3\alpha .$$

The minimax response covariances were generally higher than those presented in Appendix C. The covariance ratios were approximately

Response	Minimax/Appendix C
β	10/1
$\dot{\beta}$	1/1
I_b	10/1
$\dot{I}_b$	1/1
$\dot{\varphi} + .388\alpha$	10/1
z	1/1
$\dot{z}$	10/1

It must be pointed out that these ratios are not a fair test of the minimax. The minimax design did not include the actuator, and no $\dot{\varphi} + .388\alpha$ criteria was imposed. Further, the covariances were obtained with piecewise constant minimax controls; no attempt to smooth the control variations was made.

It is felt that under these conditions the covariance ratios are remarkably close, and the results demonstrate the soundness of the minimax procedure.

E. Anticipated Work

This subsection contains brief discussions of the current project status, preliminary conclusions, and the future work anticipated.

1. Analysis

The results presented in Appendix C of this report demonstrate that the direct-iteration technique works quite well. All but one of the failure-likelihoods produced are very low, and it is expected that the remaining likelihood will be satisfactorily reduced with a few more iterations.

It is felt that the direct-iteration technique is itself sufficient for our purposes. Further refinement of already low likelihoods with gradient techniques (PR1) would be a waste of effort.

Future analysis efforts should be directed first towards obtaining a realistic, computationally feasible bending-moment-rate expression. The above analyses employed an arbitrarily modified expression, and a more realistic expression is required if the results are to be physically significant.

This done, the direct-iteration technique can be applied to determine a controller. The two remaining analysis tasks then will be to determine the effects of amplitude-limit variations and the causes of the various peaks, sign changes, and relative gain magnitudes. The last effort is essential in that we cannot claim to have solved the control problem until the causal relations determining the behavior of its solution have been understood.

2. Simulation

Simulation tests will begin in the coming reporting period with a controller developed with the direct-iteration technique. The purposes of these tests are to check the analyses, to gain understanding of the behavior of the controlled system, to compare competitive controllers, and to reduce the controller time-histories to a physically constructable controller.

The simulation tests will be started with the vehicle model described in (QR1). It is recognized that the simulation will suffer the bending-moment-rate anomalies described in Section IIIA. This is further reason to concentrate analysis efforts on finding a realistic, computationally feasible bending-moment-rate expression.

APPENDIX A

A MODEL FOR A LAUNCH VEHICLE THAT INCLUDES DISTRIBUTED AERODYNAMIC STRIP (TRANSVERSE) FORCES

APPENDIX A

A MODEL FOR A LAUNCH VEHICLE THAT INCLUDES DISTRIBUTED AERODYNAMIC STRIP (TRANSVERSE) FORCES

By C. R. Stone

ABSTRACT

Data for the "Model Vehicle #2 are modified to exhibit aerodynamic forces distributed along the length of the vehicle. This modification eliminates unrealistic impulses in bending moment rate due to step winds. The distributed loads can be approximated by adding more dynamics to the plant representation.

INTRODUCTION

Pages 6-10 of the First Quarterly Progress Report discuss the physically unrealistic values of bending moment rate due to wind shears calculated for the "Model Vehicle #2" (Reference 1) as presented in Appendix B of the Quarterly Progress Report. The lumped parameter approximation calculates infinite bending moment rates due to step winds.

It is the purpose of this appendix to provide a modification to the plant model that will provide more realistic measures of bending moment rate. In the interest of expediency the equations of motion are modified in the simplest manner that will provide distributed loads. The equations are derived based on the assumption that at a given flight condition (dynamic pressure and Mach number) the aerodynamic load at a point on the vehicle is due solely to the motion of that point. Integrating these loads across the vehicle yields the force on a transverse strip. Herein, the unsteady aerodynamic forces are computed from Newtonian Impact Theory (Reference 2) and Piston Theory (Reference 4) in a manner that is consistent with the lumped parameter data for Model Vehicle #2 supplied by NASA (Reference 1).

Impact Theory is used to estimate the unsteady aerodynamic loads over the portion of the vehicle where there is axial symmetry. Modified first order Piston Theory is used to estimate the unsteady aerodynamic loads over the finned portion of the vehicle. Modifications consist of replacing the Mach number effect of Piston Theory with the Prandtl-Ackert and Prandtl-Glauert correction factors for supersonic and subsonic speeds. Transonically the factors are limited to 2. Fin tip leakage at supersonic speeds is estimated by using a linear variation between the tip and the Mach cone.

Consistency between Model Vehicle #2 data and the unsteady aerodynamic loads estimated by the above procedure is developed by enforcing agreement between the old and revised models for constant wind gusts.

While it may subsequently be necessary to estimate the unsteady aerodynamic loads by other by use of other theories, it does appear that Newtonian Impact and Piston Theories are the best choice for first estimates of the unsteady air loads. First, they yield local pressures as a function of the local body motion; as opposed to yielding local pressures as a functional over the entire vehicle. The point function relationship between local motion and pressure leads to simpler equations of motion than will probably be attained by more accurate theories.

Second, they are surprisingly accurate during the flight conditions where it is expected the unsteady aerodynamic effects are important. Efforts with the minimax effort to bending moment minimization show, as would be anticipated, that the problem is most difficult at the maximum dynamic pressure flight condition (page 48 of Reference 3). If compromises in the vehicle modeling must be made, they should be most accurate where the dynamic pressure is the highest. The Mach number at the highest dynamic pressure flight condition is 1.7. This is below the hypersonic regime where Impact

and Piston Theories yields excellent results. The Mach number is sufficiently high that qualitative conclusions resulting from their use should prevail and it is even expected that quantitative results would not be changed markedly.

The unsteady loads are summarized next. Equations of motion are then presented that do not include effects of time rates of change of coefficients; these should prove to be satisfactory. Following the presentation of the unsteady airload data and equations of motion needed for continuing the control synthesis there is a discussion lumping the distributed loads. The air loads and equations are then derived.

AIR LOADS

The normal air load on a transverse strip at station x is called $\tilde{t}$; it is the integral of the pressure across the vehicle at station x. The integral of $\tilde{t}$ from tail to nose would yield the total normal force. $\frac{1}{q}\frac{d\tilde{t}}{d\alpha}$ is tabulated below; q is dynamic pressure in kg/m^2, α is the angle of attack in rad, M_A is Mach number, and $\tilde{t}$ is the transverse force in kg/m.

$$\frac{1}{q}\frac{d\tilde{t}}{d\alpha} = 21.293 - 2.45x \qquad \text{for } 0.63 \le x \le 1.63$$

$$= \frac{4}{\sqrt{1-M_A^2}}\{9.17\} \qquad \text{for } M_A < \frac{\sqrt{3}}{2}, \text{ and for } 1.63 < x \le 2.54$$

$$= 8\left\{9.17 - \frac{(2M_A-\sqrt{3})}{(\sqrt{5}-\sqrt{3})}\frac{3.14-x}{\sqrt{M_A^2-1}}\right\} \qquad \text{for } \frac{\sqrt{3}}{2} \le M_A \le \frac{\sqrt{5}}{2} \text{ and for } 1.63 < x \le 2.54$$

$$= \frac{4}{\sqrt{M_A^2-1}}\left\{9.17 - \frac{3.14-x}{\sqrt{M_A^2-1}}\right\} \qquad \text{for } \frac{\sqrt{5}}{2} < M_A \text{ and for } 1.63 < x \le 2.54$$

$$\frac{1}{q}\frac{d\tilde{t}}{d\alpha} = \frac{4}{\sqrt{1-M_A^2}}\{19.22\} \quad \text{for } M_A < \frac{\sqrt{3}}{2} \quad \text{and for } 2.54 < x \leq 3.14$$

$$= 8\{19.22 - \frac{(2M-\sqrt{3})}{(\sqrt{5}-\sqrt{3})}\frac{3.14-x}{\sqrt{|M_A^2-1|}}\} \quad \text{for } \frac{\sqrt{3}}{2} \leq M_A \leq \frac{\sqrt{5}}{2} < M \quad \text{and for } 2.54 \leq x \leq 3.14$$

$$= \frac{4}{\sqrt{M_A^2-1}}\{19.22 - \frac{3.14-x}{\sqrt{M_A^2-1}}\} \quad \text{for } \frac{\sqrt{5}}{2} < M_A \quad \text{and for } 2.54 \leq x \leq 3.14$$

$$\frac{1}{q}\frac{d\tilde{t}}{d\alpha} = \frac{4}{\sqrt{1-M_A^2}}\{31.26-3.805x\} \quad \text{for } M_A < \frac{\sqrt{3}}{2} \quad \text{and for } 3.14 < x \leq 5.05$$

$$= 8\{31.26-3.805x\} \quad \text{for } \frac{\sqrt{3}}{2} \leq M_A \leq \frac{\sqrt{5}}{2} \quad \text{and for } 3.14 < x \leq 5.05$$

$$= \frac{4}{\sqrt{M_A^2-1}}\{31.26-3.805x\} \quad \text{for } \frac{\sqrt{5}}{2} < M_A \quad \text{and for } 3.14 < x \leq 5.05$$

$$= 21.6056 - 2.455x \quad \text{for } 5.05 < x \leq 8.32$$

$$= 1.1850 \quad \text{for } 8.32 < x \leq 84.08$$

$$= 15.82 - 0.448\{x-122.09\} - 0.2036\{x-122.09\}^2 \quad \text{for } 84.08 < x \leq 90.31$$

$$= 0.9875 \quad \text{for } 90.31 < x \leq 122.09$$

$$= 7.28 - 0.1830\{x-84.08\} \quad \text{for } 122.09 < x \leq 126.51$$

$$= 0.6583 \quad \text{for } 126.51 < x \leq 142.30$$

$$= 3.91\{144.86-x\} \quad \text{for } 142.30 < x \leq 144.86$$

EQUATIONS OF MOTION

Equations of motion that include the distributed airloads but do not include the effects of time rates of change of coefficients are presented.

The transition equations are

$$\begin{vmatrix} \ddot{\varphi} \\ \ddot{z} \\ \dot{\beta} \\ \dot{\varphi} \\ \dot{z} \end{vmatrix} = \begin{vmatrix} \bar{a}_{11} & a_{12} & a_{13} & a_{14} & 0 \\ \bar{a}_{21} & a_{22} & a_{23} & a_{24} & 0 \\ 0 & 0 & a_{33} & 0 & 0 \\ 1 & 0 & 0 & 0 & 0 \\ 0 & 1 & 0 & 0 & 0 \end{vmatrix} \begin{vmatrix} \dot{\varphi} \\ \dot{z} \\ \beta \\ \varphi \\ z \end{vmatrix} + \begin{vmatrix} 0 \\ 0 \\ b_3 \\ 0 \\ 0 \end{vmatrix} u + \begin{vmatrix} \bar{c}_1(\tilde{v}_w, t) \\ \bar{c}_2(\tilde{v}_w, t) \\ 0 \\ 0 \\ 0 \end{vmatrix} \qquad 2.1$$

where

$$\bar{a}_{11} = (ff)_1 \frac{1}{I_{xx}} \int_{x_T}^{x_N} \frac{d\tilde{t}}{d\alpha} \frac{(x - x_{CG})^2}{V} \, dx$$

$$a_{12} = -\frac{a_{14}}{V}$$

$$a_{13} = -\frac{F}{2I_{xx}}(x_{CG} - x_\beta) = -C_2$$

$$a_{14} = -\frac{C_{z_\alpha} q \frac{\pi}{4} D^2}{I_{xx}}(x_{CG} - x_{CP}) = -C_1$$

$$\bar{a}_{21} = (ff)_2 \frac{1}{m} \int_{x_T}^{x_N} \frac{d\tilde{t}}{d\alpha} \frac{(x - x_{CG})}{V} \, dx$$

$$a_{22} = -\frac{1}{V} \frac{C_{z_\alpha} q \frac{\pi}{4} D^2}{m} = -\frac{1}{V}\left(\frac{N'}{m}\right)$$

$$a_{23} = \frac{F}{2m}$$

$$a_{24} = +\frac{F-X}{m} + \frac{C_{z_\alpha} q \frac{\pi}{4} D^2}{m} = \frac{F-X}{m} + \frac{N'}{m}$$

$$a_{33} = -14.6$$

$$b_3 = +14.6$$

$$\bar{c}_1(\tilde{v}_w, t) = \frac{(ff)_1}{I_{xx}} \int_{x_T}^{x_N} \frac{d\tilde{t}}{d\alpha} (x - x_{CG}) \frac{v_w(x_N, t - \frac{x_N - x}{V})}{V} dx$$

$$\bar{c}_2(\tilde{v}_w, t) = \frac{(ff)_2}{m} \int_{x_T}^{x_N} \frac{d\tilde{t}}{d\alpha} \cdot \frac{v_w(x_N, t - \frac{x_N - x}{V})}{V} dx$$

$$(ff)_1 = \frac{C_1 I_{xx}}{\int_{x_T}^{x_N} \frac{d\tilde{t}}{d\alpha} (x - x_{CG}) dx}$$

$$(ff)_2 = \frac{(\frac{N}{m})'_m}{\int_{x_T}^{x_N} \frac{d\tilde{t}}{d\alpha} \frac{1}{V} dx}$$

The criteria equations are

$$\begin{vmatrix} \beta \\ \dot{\beta} \\ I_B \\ \dot{I}_B \\ S \\ \dot{z} \\ z \end{vmatrix} = \begin{vmatrix} 1 & 0 & 0 & 0 & 0 \\ d_{21} & 0 & 0 & 0 & 0 \\ d_{31} & \bar{d}_{32} & d_{33} & d_{34} & 0 \\ \bar{d}_{41} & \bar{d}_{42} & \bar{d}_{43} & \bar{d}_{44} & 0 \\ 0 & 1 & d_{53} & d_{54} & 0 \\ 0 & 0 & 0 & 1 & 0 \\ 0 & 0 & 0 & 1 & 1 \end{vmatrix} \begin{vmatrix} \beta \\ \dot{\varphi} \\ \varphi \\ \dot{z} \\ z \end{vmatrix} + \begin{vmatrix} 0 \\ e_2 \\ 0 \\ e_4 \\ 0 \\ 0 \\ 0 \end{vmatrix} u + \begin{vmatrix} 0 \\ 0 \\ \bar{f}_3(\tilde{v}_w, x, t) \\ \bar{f}_4(\tilde{v}_w, x, t) \\ f_5 v_w \\ 0 \\ 0 \end{vmatrix} + \begin{vmatrix} 0 \\ 0 \\ 0 \\ \bar{g}_4(\dot{\tilde{v}}_w, x, t) \\ 0 \\ 0 \\ 0 \end{vmatrix} \quad 2.2$$

where

$$d_{21} = a_{33}$$

$$d_{31} = M'_{\beta}$$

$$\bar{d}_{32} = \int_{x_T}^{x_N} \{ -\frac{d\tilde{t}}{d\alpha} \frac{(x' - x_{CG})}{V} (x - x') + M'(x - x')[\bar{a}_{21} + (x' - x_{CG})\bar{a}_{11}] \} dx'$$

$$d_{33} = M'_{\alpha}$$

$$d_{34} = -\frac{d_{33}}{V}$$

$$\bar{d}_{41} = d_{31}a_{33} + \bar{d}_{32}a_{13} + d_{34}a_{23}$$

$$\bar{d}_{42} = \bar{d}_{32}\bar{a}_{11} + d_{33} + d_{34}\bar{a}_{21}$$

$$d_{43} = \bar{d}_{32}a_{14} + d_{34}a_{24}$$

$$\bar{d}_{44} = \bar{d}_{32}a_{12} + d_{34}a_{22}$$

$$d_{53} = 0.338$$

$$d_{54} = -\frac{0.338}{V}$$

$$e_2 = +b_3$$

$$e_4 = +d_{31}b_3$$

$$\bar{f}_3(\tilde{v}_w,x,t) = -(ff)_6 \int_{x_T}^{x} \frac{d\tilde{t}}{d\alpha}(x - x') \frac{v_w(x_N, t - \frac{x_N - x'}{V})}{V} dx' +$$

$$+ (ff)_6 \int_{x_T}^{x} M'(x - x')\left\{ \int_{x_T}^{x_N} \frac{d\tilde{t}}{d\alpha} \frac{v_w(x_N, t - \frac{x_N - x''}{V})}{V} \cdot\cdot \right.$$

$$\left. \cdot \left[\frac{(ff)_1}{I_{xx}}(x'' - x_{CG})(x' - x_{CG}) + \frac{(ff)_2}{m} \right] dx'' \right\} dx'$$

$$\bar{f}_4(\tilde{v}_w,x,t) = \bar{d}_{32}\bar{c}_1(\tilde{v}_w,t) + d_{34}\bar{c}_2(\tilde{v}_w,t)$$

$$f_5 = +\frac{0.338}{V}$$

$$\bar{g}_4(\dot{\tilde{v}}_w,x,t) = \int_{x_T}^{x} \mu_1(x,x',t)\dot{v}_w(x_N,t - \frac{x_N - x'}{V})dx' +$$

$$+ \int_{x_T}^{x}\int_{x_T}^{x_N} \mu_2(x,x',x'',t)\dot{v}_w(x_N,t - \frac{x_N - x''}{V})dx''dx'$$

$$(ff)_6 = \frac{d_{33}}{V} \div \left\{ \int_{x_T}^{x} \left\{ - \frac{d\tilde{t}}{d\alpha} \frac{(x - x')}{V} \right\} dx' + \int_{x_T}^{x} M'(x - x') \int_{x_T}^{x_N} \frac{d\tilde{t}}{d\alpha} \frac{1}{V} \cdot \right.$$

$$\left. \cdot \left[\frac{(ff)_1}{m} (x'' - x_{CG})(x' - x_{CG}) + \frac{(ff)_2}{m} \right] dx'' \right\} dx'$$

$$\mu_1(x,x',t) = -(ff)_6 \frac{d\tilde{t}}{d\alpha}(x - x')\frac{1}{V}$$

$$\mu_2(x,x',x'',t) = \mu_3(x,x',x'',t)\ \mu_4(x',x'',t)$$

$$\mu_3(x,x',x'',t) = (ff)_6\ M'(x - x')\ \frac{d\tilde{t}}{d\alpha}$$

where M' and $\frac{d\tilde{t}}{d\alpha}$ are a function of x' and x'', respectively.

$$\mu_4(x',x'',t) = \frac{(ff)_1}{I_{xx}} (x'' - x_{CG})(x' - x_{CG}) + \frac{(ff)_2}{m}$$

The sources for all data except unsteady air load derivative ($\frac{d\tilde{t}}{d\alpha}$) and the running mass M' have been called out in Appendix B of the First Quarterly Progress Report. $\frac{d\tilde{t}}{d\alpha}$ is tabulated in the previous part of this Appendix. The running mass M' can be obtained by use of pg 56 of reference 1 and the total mass (m) and center of gravity data.

LUMPING THE LOADS

Equations 2.1 and 2.2 previously presented may be revised to replace the distributed air loads with equivalent lumped-parameter dynamic load build-up functions. This would permit replacing the lumped parameter representation that has been used with one of higher order that correctly represents the distributed air load. The revised equations would not display impulses in bending moment rate due to step winds.

Development of the lumped parameter models for the unsteady air loads has just been started. This discussion will therefore necessarily just indicate how the lumping will be accomplished. The step responses (due to a wind gust) for $\bar{c}_1(\tilde{v}_w,t)$, $\bar{c}_2(\tilde{v}_w,t)$, $\bar{f}_3(v_w,x,t)$ $\bar{f}_4(\tilde{v}_w,x,t)$, and $\bar{g}_4(\dot{\tilde{v}}_w,x,t)$ will be determined by use of the unsteady air load data previously presented. The step responses will be approximated by lumped-parameter dynamic models and the lumped-parameter dynamics will be added to the equations of motion.

The estimation of the lumped-parameter model for $\bar{c}_2(\tilde{v}_w,t)$ will be used to illustrate the procedure.

Figure A-1 presents the unsteady air load at the high dynamic pressure flight condition. Integrating this and normalizing yields the normalized step response for $\bar{c}_2$ as presented in Fig. A-2. The rapid changes in load are due to the nose cone, first and second cone frustrum transition sections, and the fins.

The lumping problem is thus the approximation of the step response of Fig. A-2 with dynamics that have a similar step response. Once the form of the approximating dynamics have been determined, optimization of the parameters can be accomplished in a straightforward manner. Figure A-2 (and the geometry of the vehicle) indicate the step response might be approximated by the superposition of lags at 0.050, 0.115,

and 0.280 sec. Dr. Skelton estimates that increases in computational times for delays of this magnitude are about equivalent to 25 orders of differential equation. Hence, a differential approximation to Fig. A-2 will be sought. It seems obvious that Pade approximates (pp. 547-551 of Reference 5) should be used. Superpostion of 0.4 of a first over second Pade approximate at 0.28 sec and 0.6 of a 0.1 sec lag yields an approximation that is good to within 20% but the error is plus and minus near 0.28 sec. This indicates that a Pade approximate of at least third over fourth must be used to obtain qualitatively correct results.

Future plans include developing satisfactory approximations.

ESTIMATION OF UNSTEADY AIR LOADS

The sources of and approximations to the acrodynamic theories are discussed first. These results are then used to estimate the loads on the two and three dimensional parts of the vehicle.

AERODYNAMIC THEORIES

Piston theory is the basis for estimating the loads over the two-dimensional (finned) regions and impact theory is used for the three-dimensional axially symmetric regions.

Two Dimensional

First order piston theory (reference 4) states that the unsteady pressure difference Δp across a two-dimensional surface at high Mach number is given by

$$\Delta p = \frac{4}{M_A} q\alpha \qquad 4.1$$

The average steady-state Δp for thin airfoils at supersonic speeds is given by the Prandtl-Ackert expression

$$\Delta p = \frac{4}{\sqrt{M_A^2 - 1}} q\alpha \qquad 4.2$$

and for subsonic speeds by the Prandtl-Glauert

$$\Delta p = \frac{C_{L_{\alpha_0}}}{\sqrt{1-M_A}} 2\, q\alpha \qquad 4.3$$

Considering the fin aspect ratio and present intentions it seems reasonable to take $C_{L_{\alpha_0}} = 4$.

Equations 4.2 and 4.3 agree at Mach one. Equations 4.1 and 4.2 are about equal at high Mach numbers. It thus appears reasonable to replace M_A in equation 4.1 by $\sqrt{|M_A^2-1|}$.

At unity Mach number $\frac{2}{\sqrt{|M_A^2-1|}}$ goes to infinity and it is larger at all transonic speeds than experiments show. The Prandtl correction factors will be arbitrarily truncated at 2. Hence, the final two-dimensional piston theory pressure difference will be taken as

$$\Delta p = \begin{cases} \dfrac{4}{\sqrt{|M_A^2-1|}}\, q\alpha & \text{if } \dfrac{1}{\sqrt{|M_A^2-1|}} < 2 \\ 8\, q\alpha & \text{if } \dfrac{1}{\sqrt{|M_A^2-1|}} \geq 2 \end{cases} \qquad 4.4$$

Tip leakage is assumed to be lumped in $C_{L_{\alpha_0}} = 4$ for $M_A < \sqrt{3}/2$. For $M_A > \sqrt{5}/2$ tip leakage is accounted for by linearly reducing the Δp calculated by equation 4.4 by the inboard Mach line and the fin tip, i.e.,

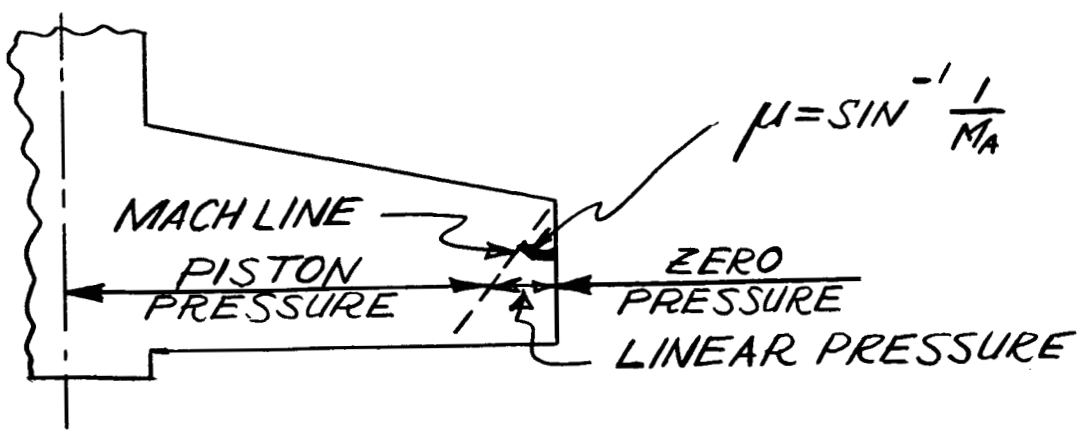

For $\sqrt{3}/2 < M_A < \sqrt{5}/2$ tip leakage is assumed to vary linearly.

Three Dimensional

The air loads on the axially symmetric and engine shroud parts of the body are calculated from impact theory (reference 2) which estimates the pressure on unshielded portions (unobstructed line of sight to the relative wind) as

$$p = \rho V_N^2 \qquad 4.5$$

where

ρ is the air density

V_N air velocity normal to the surface.

The pressure on shielded portions is taken as zero.

VEHICLE DIMENSIONS

The vehicle dimensions are assumed to be those presented in Fig. A-3; this comes from page 53 of reference 1.

Impact theory is used to estimate air loads on the parts of the vehicle except for those between 1.63 and 5.05. Two two-dimensional area excludes the 396" strip between body stations 1.63 and 2.54.

TWO DIMENSIONAL

Application of the piston theory results presented in equation 4.4 to the geometry just defined is immediate. The results are presented in the equations for body stations 1.63 to 5.05 under AIR LOADS.

THREE DIMENSIONAL

The application of impact theory to unsteady air loads estimation is presented in detail in order to display some assumptions made. The order of presentation is nose cone, cylindrical sections, transition sections, and shrouds and aft body.

Nose Cone

The surface of the cone in rectangular coordinates

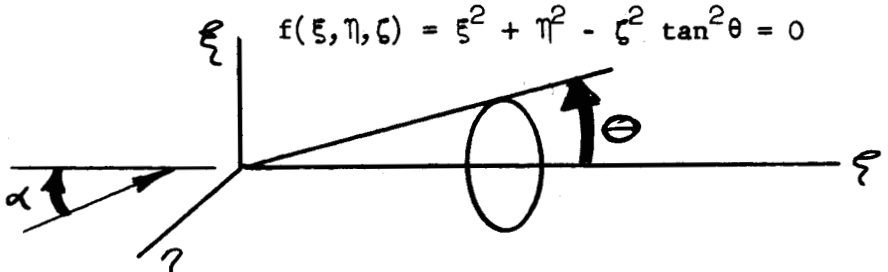

$$f(\xi,\eta,\zeta) = \xi^2 + \eta^2 - \zeta^2 \tan^2\theta = 0 \qquad 4.6$$

To integrate pressures around the cone it is desirable to use polar coordinates

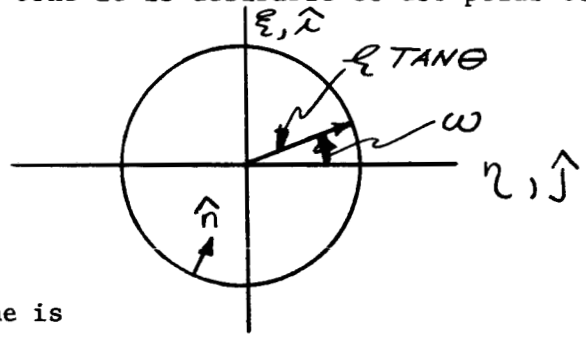

$$\xi = \zeta \sin\omega \tan\theta$$

$$\eta = \zeta \cos\omega \tan\theta. \qquad 4.7$$

The unit inward normal to the cone is

$$\hat{n} = \left|\frac{\nabla f}{\nabla f}\right| = \frac{-\xi\hat{i} - \eta\hat{j} + \zeta\tan^2\theta\hat{k}}{\sqrt{\xi^2 + \eta^2 + \zeta^2 \tan^4\theta}}$$

$$= -\cos\theta \sin\omega\hat{i} - \cos\theta \cos\omega\hat{j} + \sin\theta\hat{k} \qquad 4.8$$

The wind vector is taken in the ξ - ζ plane so

$$\bar{V} = V \sin\alpha\hat{i} + V \cos\alpha\, \hat{k} \qquad 4.9$$

The velocity and pressure normal to the cone are

$$\bar{V}_n = (\bar{V}\cdot \hat{n})\hat{n} = V_n\hat{n} = V(-\sin\alpha \cos\theta \sin\omega + \cos\alpha \sin\theta)\hat{n} \qquad 4.10$$

$$(\bar{V} \cdot \hat{n})^2 = \frac{V^2(\sin^2\omega \sin^2\alpha - 2\sin\omega \sin\alpha \cos\alpha \tan\theta + \cos^2\alpha \tan^2\theta)}{\sec^2\theta} \qquad 4.11$$

$$\bar{p} = \rho V_n^2 \hat{n} \qquad 4.12$$

For $\bar{p}$ it was assumed that $|\alpha| \leq |\theta|$

so the formula is valid around the entire cone; no part of the surface lies in the shadow.

The ζ running load $(\tilde{t})$ in the ξ direction is the integral of the component of pressure in the ξ direction

$$\tilde{t} = -\int_{\zeta\tan\theta}^{-\zeta\tan\theta} \bar{p} \cdot \tilde{i}\, d\eta + \int_{-\zeta\tan\theta}^{\zeta\tan\theta} \bar{p} \cdot \hat{i}\, d\eta$$

$$= +2\, q\frac{\sin\theta}{\sec^2\theta}\, \zeta\left\{ \int_0^{\pi} f(\alpha,\theta,\omega)\, d\omega - \int_{\pi}^{2\pi} f(\alpha,\theta,\omega)\, d\omega \right\} \qquad 4.13$$

where

$$f(\alpha,\theta,\omega) = -\sin^2\alpha\sin^4\omega + 2\sin\alpha\cos\alpha\tan\theta\sin^3\omega - \cos^2\alpha\tan^2\theta\sin^2\omega$$

The integral

$$\int_{\omega_L}^{\omega_u} f(\alpha,\theta,\omega)\, d\omega = -\sin^2\alpha\left\{ -\frac{\sin^3\omega\cos\omega}{4} - \frac{3}{8}\cos\omega\sin\omega + \frac{3}{8}\omega \right\}_{\omega_L}^{\omega_u}$$

$$+ 2\sin\alpha\cos\alpha\tan\theta\left\{-\tfrac{1}{3}\cos\omega(\sin^2\omega + 2)\right\}_{\omega_L}^{\omega_u}$$

$$-\cos^2\alpha\tan^2\theta\left\{-\tfrac{1}{2}\cos\omega\sin\omega + \frac{\omega}{2}\right\}_{\omega_L}^{\omega_u} \qquad 4.14$$

Hence, for the nose cone

$$\tilde{t} = q\zeta\, \frac{16}{3}\, \frac{\sin^2\theta}{\sec\theta}\, \sin 2\alpha \qquad 4.15$$

$$\frac{d\tilde{t}}{d\alpha} = q\zeta\, \frac{32}{3}\, \frac{\sin^2\theta}{\sec\theta}\, \cos 2\alpha \qquad 4.16$$

Figure A-3 indicates the nose cone is between

$142.30 < x \leq 144.86$

The cone semi-angle θ is

$$\theta = \tan^{-1} \frac{\frac{110}{39.37}}{2.56} \cong 47.6°$$

so for small α

$$\frac{1}{q} \frac{d\tilde{t}}{d\alpha} = (3.91)(144.86-x) = 566.4026-3.91x \qquad 4.17$$

for

$142.30 < x \leq 144.86$

Cylindrical Sections

The surfaces of the cylinders in rectangular coordinates are taken as

$$f(\xi, \eta, \zeta) = 0 = \xi^2 + \eta^2 - R^2 \qquad 4.18$$

The surfaces in polar coordinates are

$$\xi = R \sin\omega \qquad 4.19$$

$$\eta = R \cos\omega$$

The unit inward normal to a cylinder is

$$\hat{n} = \frac{\nabla f}{|\nabla f|} = \frac{-\xi\hat{i} - \eta\hat{j}}{\sqrt{\xi^2 + \eta^2}}$$

$$= -\sin\omega\hat{i} - \cos\omega\hat{j} \qquad 4.20$$

The wind vector is taken in the ξ - ζ plane so $\bar{V} = V\sin\alpha\hat{i} + V\cos\alpha\,\hat{k}$

The velocity and pressure normal to a cylinder are

$$\bar{V}_n = (\bar{V} \cdot \hat{n})\hat{n} = V_n\hat{n} = (-V\sin\alpha\,\sin\omega)\hat{n} \tag{4.21}$$

$$(\bar{V} \cdot \hat{n})^2 = V^2\sin^2\alpha\,\sin^2\omega \tag{4.22}$$

$$\bar{p} = \begin{cases} 0 & \text{if } \sin\alpha\,\sin\omega \geq 0 \\ \rho V_n^{\,2}\hat{n} = \rho V^2\sin^2\alpha\sin^2\omega\hat{n} & \text{if } \sin\alpha\,\sin\omega \leq 0 \end{cases} \tag{4.23}$$

The pressure formula indicates that pressures on the backside is taken as zero.

The ζ running load in the ξ direction is the integral of the component of pressure in the ξ direction

$$\tilde{t} = -\int_R^{-R} \bar{p} \cdot \hat{i}\,d\eta + \int_{-R}^{R} \bar{p} \cdot \hat{i}\,d\eta$$

$$= +R\int_0^{\pi} \bar{p} \cdot \hat{i}\,\sin\omega\,d\omega - R\int_{\pi}^{2\pi} \bar{p} \cdot \hat{i}\,\sin\omega\,d\omega \tag{4.24}$$

If $\alpha > 0$, the first integral on the right is zero; if $\alpha < 0$, the second integral on the right is zero.

So for $\alpha > 0$

$$\tilde{t} = q\,D\,\sin^2\alpha\int_{\pi}^{2\pi}\sin^4\omega d\omega$$

$$= q\,D\,\sin^2\alpha\left\{-\frac{\sin^3\omega\,\cos\omega}{4} - \frac{3}{8}\cos\omega\,\sin\omega + \frac{3}{8}\omega\right\}_{\pi}^{2\pi}$$

$$= q\,D\,\frac{3\pi}{8}\sin^2\alpha \tag{4.25}$$

for $\alpha \geq 0$

For any α

$$\tilde{t} = qD \frac{3\pi}{8} \sin^2\alpha \, \text{sign}\alpha \qquad 4.26$$

This infamous result will be linearized and agreement will be enforced at 0.1 rad so

$$\frac{1}{q}\frac{d\tilde{t}}{d\alpha} \cong D \frac{0.3\pi}{8} \qquad 4.27$$

From this and Fig. A-3,

$$\frac{1}{q}\frac{d\tilde{t}}{d\alpha} = 0.6583 \quad \text{for } 126.51 < x \leq 142.20 \qquad 4.28$$

$$\frac{1}{q}\frac{d\tilde{t}}{d\alpha} = 0.9875 \quad \text{for } 90.31 < x \leq 122.09 \qquad 4.29$$

$$\frac{1}{q}\frac{d\tilde{t}}{d\alpha} = 1.1850 \quad \text{for } 8.32 < x \leq 84.08 \qquad 4.30$$

Transition Sections

The difference in the impact pressure formulae between the cone furstrum transition sections and the nose cone is in the shielding on the former.

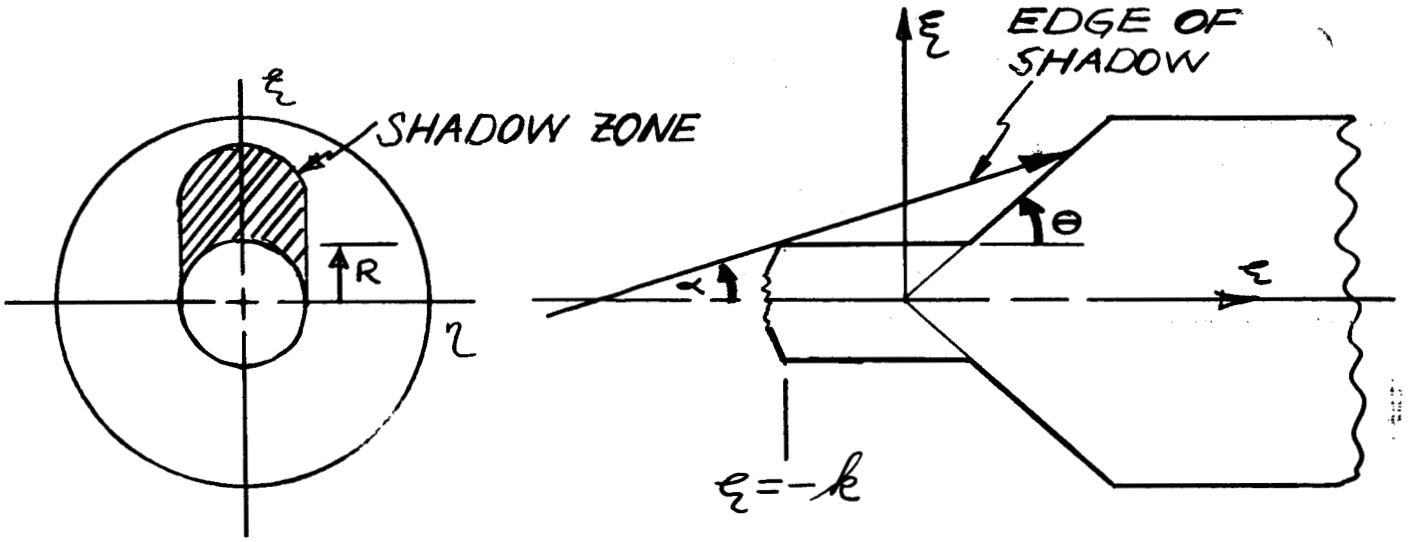

Again assuming the cone angle is greater than the angle of attack ($\theta > \alpha$), it is seen that the nose cone formula (4.13) previously developed can be used except the area of integration should not include the shadow zone of the sketch.

The edge of the shadow is

$$\eta^2 + (\xi - [k + \zeta]\tan\alpha)^2 - R^2 = 0 \qquad 4.31$$

The polar coordinates of the surface of the cone are

$$\xi = \zeta \sin\omega \tan\theta$$

$$\eta = \zeta \cos\omega \tan\theta \qquad 4.32$$

Thus, the intersection of the edge of the shadow and the cone frustrum is given by

$$\omega_s = \sin^{-1} \frac{\zeta^2\tan^2\theta + [k + \zeta]^2 \tan^2\alpha - R^2}{2\zeta[k + \zeta]\tan\alpha \tan\theta} \qquad 4.33$$

where $0 \leq \omega_s \leq \pi/2$.

This and equation 4.13 yield

$$\tilde{t} = 2q \frac{\sin\theta}{\sec^2\theta} \zeta\{\int_0^{\pi} f(\alpha,\theta,\omega)d\omega - \int_{\pi}^{2\pi} f(\alpha,\theta,\omega)d\omega - \int_{\omega_s}^{\pi-\omega_s} f(\alpha,\theta,\omega)d\omega\} \qquad 4.34$$

This could be differentiated with respect to α but it is sufficient for present purposes to develop numerical results. As for the cylinder, it will be assumed adequate to linearize and to take the derivative such that $\tilde{t}$ is correct at an angle of attack of 0.1 rad.

$$\tilde{t} = q\zeta\{\frac{16}{3} \frac{\sin^2\theta}{\sec\theta} \sin2\alpha[+1 - \frac{1}{4}\cos\omega_s(\sin^2\omega_s + 2)]$$

$$+ 2 \frac{\sin\theta}{\sec^2\theta} \sin^2\alpha[\sin2\omega_s(\frac{1}{4}\sin^2\omega_s + \frac{3}{8}) + \frac{3}{8}(\pi - 2\omega_s)]$$

$$+ \sin^3\theta \cos^2\alpha[\sin2\omega_s + \pi - 2\omega_s]\} \qquad 4.35$$

There are two cone frustrums to which the above formulae (equations 4.33 and 4.35) are to be applied. Figure A-3 puts the front one between 122.09 and 125.51, and the aft one between 84.08 and 90.31. The sketch below (taken from Fig. A-3) shows that the aft cone frustrum is affected only by the cylindrical section between stations 90.31 and 122.09; the cylinder between 126.51 m and 142.30 m does not shadow the aft cone frustrum.

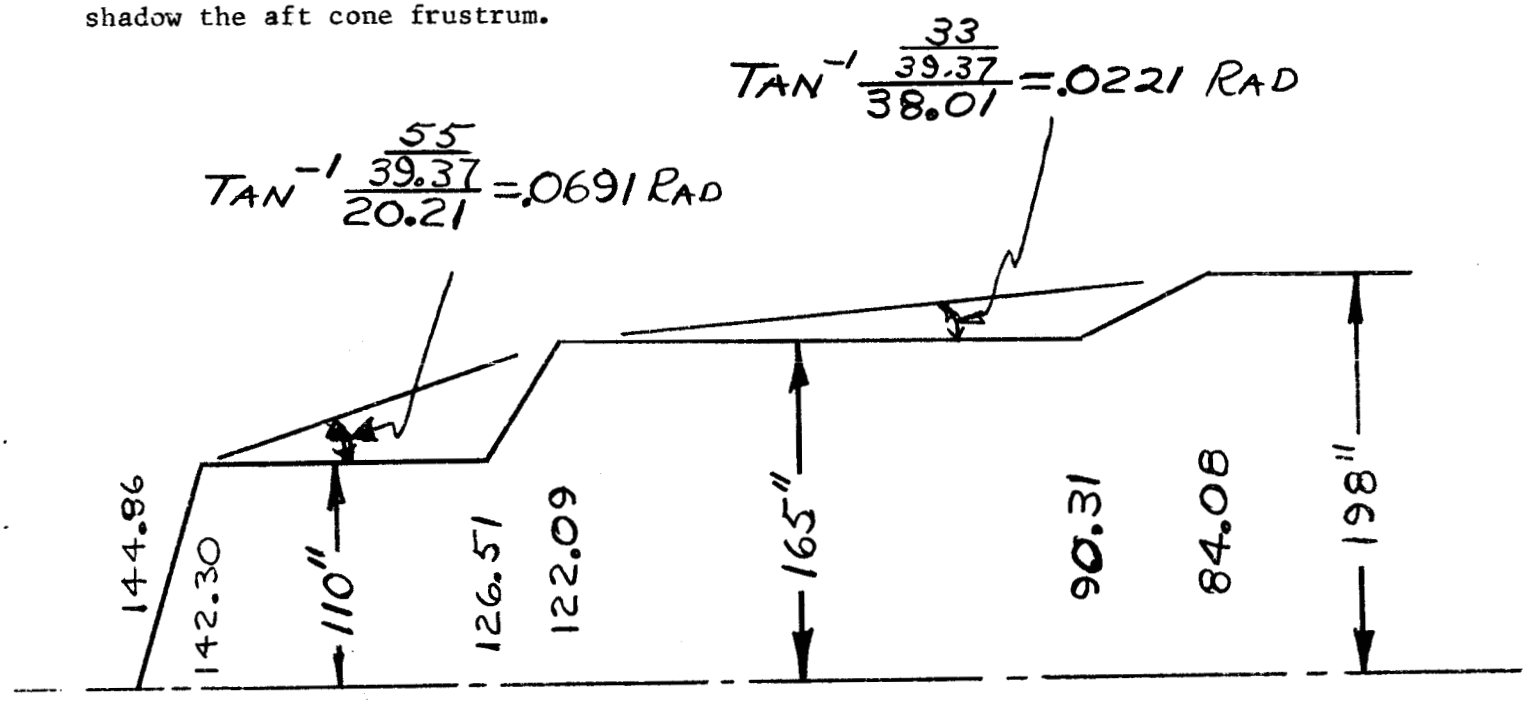

The sketch and equations 4.33 and 4.35 yield

x	ζ	ω_s	$\frac{1}{q}\frac{d\tau}{d\alpha}$
m	m	deg	
126.51	8.84	16.45	12.04
125.04	10.31	30.90	13.65
123.56	11.79	43.20	15.02
122.09	13.26	54.40	15.82
90.31	31.15	22.40	6.14
88.23	33.23	27.40	6.52
86.16	35.30	31.70	6.90
84.08	37.38	34.70	7.28

These data can be approximated by

$$\frac{1}{q}\frac{d\tilde{t}}{d\alpha} = 15.82 - 0.448\{x - 122.09\} - 0.2036\{x - 122.09\}^2 \qquad 4.36$$

for $122.09 < x \leq 126.51$ and

$$\frac{1}{q}\frac{d\tilde{t}}{d\alpha} = 7.28 - 0.1830\{x - 84.08\} \qquad 4.37$$

for $84.08 < x \leq 90.31$

Engine Shrouds and Aft Body

The shrouds are assumed to be cones centered about the control engines. This permits estimating the loads (less the fin loads) by use of the cone and cylinder formulae if the angles ω_o, ω_1, ω_2, ω_3, and ω_4 are known.

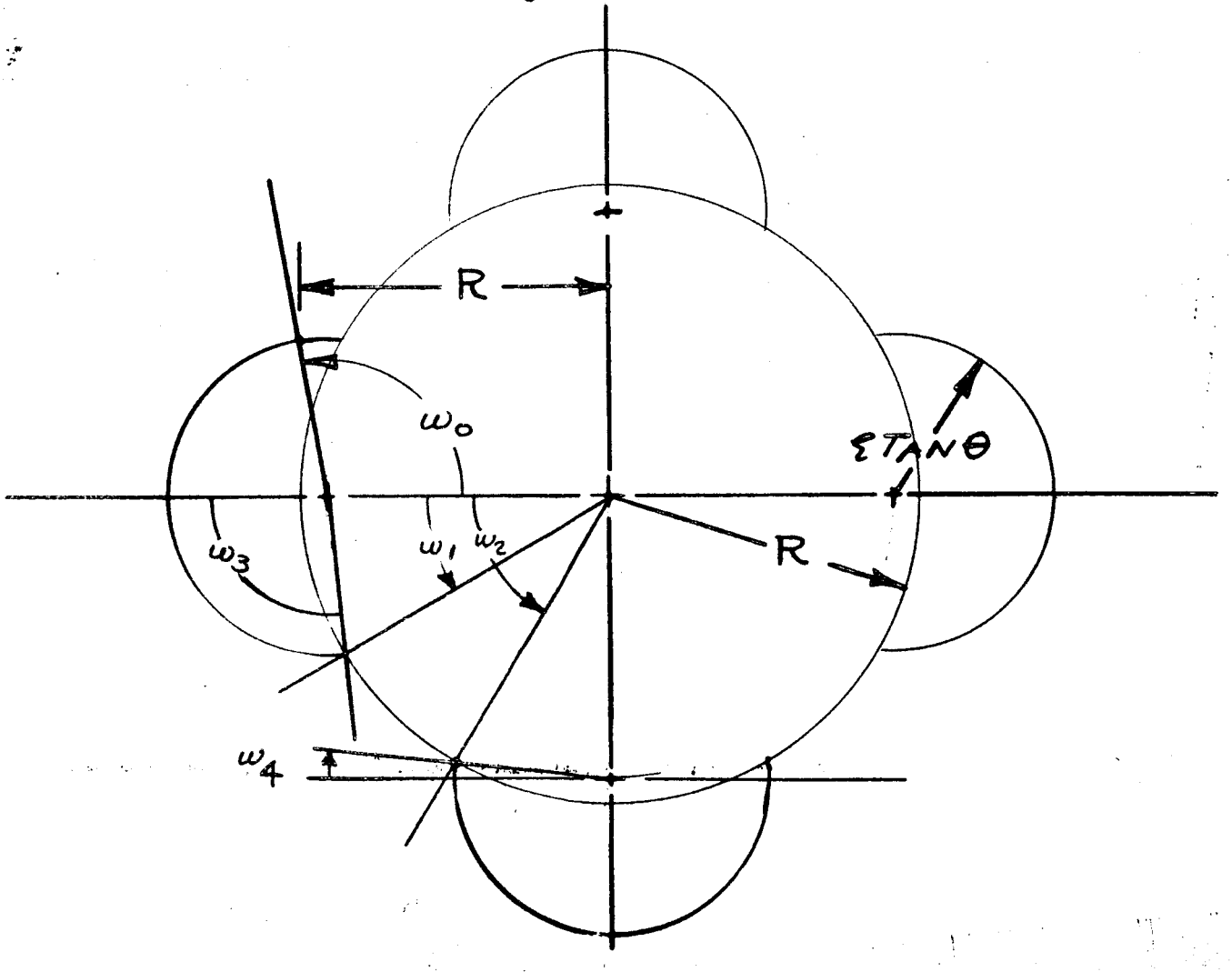

It is assumed the crosswise component of the wind is coming from below. The upward pressures on the cones (4.38) and the cylinder (4.39) are given by

$$\tilde{t} = 2q \frac{\sin\theta}{\sec^2\theta} \zeta \left\{ + \int_{\omega_o}^{\pi} 2 - \int_{\pi}^{\pi+\omega_3} 2 + (\text{sign}\omega_4) \int_{0}^{\omega_4} 2 - \int_{\pi}^{2\pi+1} \right\} f(\alpha,\theta,\omega)\, d\omega \qquad 4.38$$

$$\tilde{t} = q2R \sin^2\alpha \int_{\pi+\omega_1}^{\pi+\omega_2} \sin^4\omega \, d\omega$$

$$= q\tfrac{1}{4}R \sin^2\alpha \left\{ -\frac{1}{16} \sin 4\omega_1 + \frac{3\pi}{12} - \frac{3}{4}\omega_1 \right\} \qquad 4.39$$

The above will be evaluated at an angle of attack of 0.1 rad and the assumption will be made again that the derivatives are linear and agree at 0.1 rad. At 0.1 rad the top of the side cones between the body and the horizontal tangent is shielded by the side of 396" section. The top of the cylinder and the entire top engine shroud are shielded from the air blast.

Impact pressures will be determined at four equidistant points along the cone shrouds and aft cylindrical section.

x	ζ	$\frac{1}{q}\frac{d\tilde{t}}{d\alpha}$	ω_o	ω_1	ω_2	ω_3	ω_4
m	m		deg	deg	deg	deg	deg
8.320	1.352	0.0	180.00	.	.	0.0	-90.00
5.777	3.915	6.91	110.25			76.5	-13.5
3.193	6.479	13.38	102.08			89.35	- 0.65
0.630	9.042	19.68	98.62			97.65	+ 7.65
8.320	1.352	1.180		00.00	90.00		
6.390	3.279	0.8160		10.50	79.50		
4.470	5.205	0.5930		17.60	72.40		
2.540	7.132	0.3544		26.60	63.40		

The top data are for the engine shrouds and the lower are for the cylinder. These loads were combined to develop the load equations for $0.63 < x < 1.63$ and for $5.05 < x < 8.32$. The equations are presented in the AIR LOADS section.

DERIVATION OF THE EQUATIONS OF MOTION

This development is considered as a modification to that presented in Appendix B of the First Quarterly Progress Report. All symbols are the same as used therein except as noted.

Equation 15 modified to provide an indication of the local angle of attack is

$$\alpha(x,t) = \frac{V_w(x,t)}{V} + \varphi - \frac{\dot{z}}{V} + \frac{(x - x_{CG})}{V}\dot{\varphi} \qquad 5.1$$

Assuming the wind is stationary in space and using an average vehicle speed permits rewriting the wind as

$$v_w(x,t) = v_w(x_N, t - \frac{x_N - x}{V}) \qquad 5.2$$

where

x_N is the longitudinal coordinate at the vehicle nose.

The pitch (13) and heave (14) equations become

$$\ddot{\varphi} = \frac{1}{I_{xx}} \int_{x_T}^{x_N} \frac{d\tilde{t}(x)}{d\alpha} \alpha(x,t)\{x - x_{CG}\}dx - C_2\beta \qquad 5.3$$

$$\ddot{z} = \frac{F-X}{m}\varphi + \frac{F}{2m}\beta + \frac{1}{m}\int_{x_T}^{x_N} \frac{d\tilde{t}(x)}{d\alpha}\alpha\, dx \qquad 5.4$$

where $\frac{d\tilde{t}(x)}{d\alpha}$ is the unsteady air load derivative (tabluated in the AIR LOADS section).

The state representation 16 becomes equations 5.5.

$$\begin{vmatrix} \ddot{\varphi} \\ \ddot{z} \\ \dot{\beta} \\ \dot{\varphi} \\ \dot{z} \end{vmatrix} = \begin{vmatrix} \bar{a}_{11} & a_{12} & a_{13} & a_{14} & 0 \\ \bar{a}_{21} & a_{22} & a_{23} & a_{24} & 0 \\ 0 & 0 & a_{33} & 0 & 0 \\ 1 & 0 & 0 & 0 & 0 \\ 0 & 1 & 0 & 0 & 0 \end{vmatrix} \begin{vmatrix} \dot{\varphi} \\ \dot{z} \\ \beta \\ \varphi \\ z \end{vmatrix} + \begin{vmatrix} 0 \\ 0 \\ b_3 \\ 0 \\ 0 \end{vmatrix} u + \begin{vmatrix} \bar{c}_1(\tilde{v}_w, t) \\ \bar{c}_2(\tilde{v}_w, t) \\ 0 \\ 0 \\ 0 \end{vmatrix} \quad (5.5)$$

where

$$\bar{a}_{11} = (ff)_1 \frac{1}{I_{xx}} \int_{x_T}^{x_N} \frac{d\tilde{t}}{d\alpha} \frac{(x - x_{CG})^2}{V} dx$$

$$a_{12} = -\frac{a_{14}}{V}$$

$$a_{13} = -\frac{F}{2I_{xx}} (x_{CG} - x_\beta) = -C_2$$

$$a_{14} = -\frac{C_{z_\alpha} q \frac{\pi}{4} D^2}{I_{xx}} (x_{CG} - x_{CP}) = -C_1$$

$$\bar{a}_{21} = (ff)_2 \frac{1}{m} \int_{x_T}^{x_N} \frac{d\tilde{t}}{d\alpha} \frac{(x - x_{CG})}{V} dx$$

$$a_{22} = -\frac{1}{V} \frac{C_{z_\alpha} q \frac{\pi}{4} D^2}{m} = -\frac{1}{V}\left(\frac{N'}{m}\right)$$

$$a_{23} = \frac{F}{2m}$$

$$a_{24} = +\frac{F-X}{m} + \frac{C_{z_\alpha} q \frac{\pi}{4} D^2}{m} = \frac{F-X}{m} + \frac{N'}{m}$$

$$a_{33} = -14.6$$

$$b_3 = +14.6$$

$$\bar{c}_1(\tilde{v}_w,t) = \frac{(ff)_1}{I_{xx}} \int_{x_T}^{x_N} \frac{d\tilde{t}}{d\alpha}(x - x_{CG}) \frac{v_w(x_N, t - \frac{x_N - x}{V})}{V} dx$$

$$\bar{c}_2(\tilde{v}_w,t) = \frac{(ff)_2}{m} \int_{x_T}^{x_N} \frac{d\tilde{t}}{d\alpha} \frac{v_w(x_N, t - \frac{x_N - x}{V})}{V} dx$$

$$(ff)_1 = \frac{C_1 I_{xx}}{\int_{x_T}^{x_N} \frac{d\tilde{t}}{d\alpha}(x - x_{CG})dx}$$

$$(ff)_2 = \frac{(\frac{N}{m}')m}{\int_{x_T}^{x_N} \frac{d\tilde{t}}{d\alpha} \frac{1}{v} dx}$$

x_T = body station at tail

x_N = body station at nose

The quantities $(ff)_1$ and $(ff)_2$ are fudge factors to produce consistency between the Model Vehicle #2 data and the estimated $\frac{d\tilde{t}}{d\alpha}$. Under other situations the fudge factors might be used to provide consistency between steady-state wind tunnel data and unsteady theoretical data.

The modifications to the components of the state on which there are criteria are similarly developed. Only the bending computations of equations 19 of the First Quarterly Progress Report are affected.

The bending moments due to engine deflection (M_E), aerodynamic forces (M_A), and inertial forces (M_I) are given by

$$M_E(x) = -R'(x - x_\beta)\beta \tag{5.6}$$

$$M_A(x) = -\int_{x_T}^{x} \frac{d\tilde{t}}{d\alpha}\,\alpha(x',t)(x - x')dx' \tag{5.7}$$

$$M_I(x) = \int_{x_T}^{x} M'\ddot{\tau}(x - x')dx' \tag{5.8}$$

where

$M' = M'(x)$ is the mass density and

$$\ddot{\tau}(x) = \ddot{z} + (x - x_{CG})\ddot{\Phi} \tag{5.9}$$

is the local acceleration.

Hence,

$$I_B(x) = M_E(x) + M_A(x) + M_I(x) = -R'(x - x_\beta)\beta$$

$$+ \left\{(ff)_3 \int_{x_T}^{x} M'(x - x')[a_{23} + (x' - x_{CG})a_{13}]dx'\right\}\beta$$

$$+ \left\{\int_{x_T}^{x} - \frac{d\tilde{t}}{d\alpha}\frac{(x' - x_{CG})}{V}(x - x') + M'(x - x')[\bar{a}_{21} + (x' - x_{CG})\bar{a}_{11}]\right\}dx'\Big\}\dot{\Phi}$$

$$+ \left\{(ff)_4\int_{x_T}^{x} - \frac{d\tilde{t}}{d\alpha}(x - x') + M'(x - x')[a_{24} + (x' - x_{CG})a_{14}]\right\}dx'\Big\}\Phi \quad +$$

$$+ \left\{(ff)_5 \int_{x_T}^{x} \left\{ \frac{d\tilde{t}}{d\alpha} \frac{(x - x')}{V} + M'(x - x')[a_{22} + (x' - x_{CG})a_{12}] \right\} dx' \right\} \dot{z}$$

$$+ \left\{ -(ff)_6 \int_{x_T}^{x} \left\{ \frac{d\tilde{t}}{d\alpha} (x - x') \frac{v_w(x_N, t - \frac{x_N - x'}{V})}{V} \right\} dx' \right.$$

$$+ \left\{(ff)_6 \int_{x_T}^{x} M'(x - x') \left\{ \int_{x_T}^{x_N} \frac{d\tilde{t}(x'')}{d\alpha} \frac{v_w(x_N, t - \frac{x_N - x''}{V})}{V} \right. \right.$$

$$\left. \left. \cdot \left[\frac{(ff)_1}{I_{xx}} (x'' - x_{CG})(x' - x_{CG}) + \frac{(ff)_2}{m} \right] dx'' \right\} dx'$$

$$= d_{31}\beta + \bar{d}_{32}\dot{\varphi} + d_{33}\varphi + d_{34}\dot{z} + \bar{f}_3(\tilde{v}_w, x, t) \qquad 5.10$$

where

$$(ff)_3 = \frac{d_{31} + R'(x - x_\beta)}{\int_{x_T}^{x_N} M'(x - x')[a_{23} + (x' - x_{CG})a_{13}] dx'}$$

$$\bar{d}_{32} = \left\{ \int_{x_T}^{x} \left\{ - \frac{d\tilde{t}}{d\alpha} \frac{(x' - x_{CG})}{V} (x - x') + M'(x - x')\left[\bar{a}_{21} + (x' - x_{CG})\bar{a}_{11}\right] \right\} dx' \right.$$

$$(ff)_4 = \frac{d_{33}}{\int_{x_T}^{x_N} \left\{ - \frac{d\tilde{t}}{d\alpha} (x - x') + M'(x - x')\left[a_{24} + (x' - x_{CG})a_{14}\right] \right\} dx'}$$

$$(ff)_5 = \frac{d_{34}}{\int_{x_T}^{x} \left\{ \frac{d\tilde{t}}{d\alpha} \frac{(x - x')}{V} + M'(x - x')\left[a_{22} + (x' - x_{CG})a_{12}\right] \right\} dx'}$$

$$\tilde{f}_3(\tilde{v}_w, x, t) = -(ff)_6 \int_{x_T}^{x} \left\{ \frac{d\tilde{t}}{d\alpha} (x - x') \frac{v_w(x_N, t - \frac{x_N - x'}{V})}{V} \right\} dx' +$$

$$+ (ff)_6 \int_{x_T}^{x} M'(x - x') \left\{ \int_{x_T}^{x_N} \frac{d\tilde{t}}{d\alpha} \frac{v_w(x_N, t - \frac{x_N - x''}{V})}{V} \cdot \right.$$

$$\left. \cdot \left[\frac{(ff)_1}{I_{xx}} (x'' - x_{CG})(x' - x_{CG}) + \frac{(ff)_2}{m} \right] dx'' \right\} dx'$$

$$(ff)_6 = f_3 \div \left\{ \int_{x_T}^{x} -\left\{ \frac{d\tilde{t}}{d\alpha} \frac{(x - x')}{V} \right\} dx' + \int_{x_T}^{x} M'(x - x') \left\{ \int_{x_T}^{x_N} \frac{d\tilde{t}(x'')}{d\alpha} \frac{1}{V} \right.\right.$$

$$\left.\left. \cdot \left[\frac{(ff)_1}{I_{xx}} (x'' - x_{CG})(x' - x_{CG}) + \frac{(ff)_2}{m} \right] dx'' \right\} dx' \right\}$$

Differentiating 5.10 yields the bending moment rate equation

$$\dot{I}_B = \bar{d}_{41}\beta + \bar{d}_{42}\dot{\varphi} + \bar{d}_{43}\varphi + \bar{d}_{44}\dot{z} + e_4 u \qquad 5.11$$

$$+ \bar{f}_4(\tilde{v}_w, x, t) + \bar{g}_4(\dot{\tilde{v}}_w, x, t)$$

where

$$\bar{d}_{41} = d_{31}a_{33} + \bar{d}_{32}a_{13} + d_{34}a_{23} + \dot{d}_{31}$$

$$\bar{d}_{42} = \bar{d}_{32}\bar{a}_{11} + d_{33} + d_{34}\bar{a}_{21} + \dot{\bar{d}}_{32}$$

$$\bar{d}_{43} = \bar{d}_{32}a_{14} + d_{34}a_{24} + \dot{d}_{33}$$

$$\bar{d}_{44} = \bar{d}_{32}a_{12} + d_{34}a_{22} + \dot{d}_{34}$$

$$\bar{f}_4(\tilde{v}_w,x,t) = \bar{d}_{32}\bar{c}_1(\tilde{v}_w,t) + d_{34}\bar{c}_2(\tilde{v}_w,t)$$

$$+ \int_{x_T}^{x} \dot{\mu}_1(x,x',t)v_w(x_N,t - \frac{x_N - x'}{V})\,dx'$$

$$+ \int_{x_T}^{x}\int_{x_T}^{x_N} \dot{\mu}_2(x,x',x',t)v_w(x_N,t - \frac{x_N - x''}{V})dx''dx'$$

$$\bar{g}_4(\dot{\tilde{v}}_w,x,t) = \int_{x_T}^{x} \mu_1(x,x',t)\dot{v}_w(x_N,t - \frac{x_N - x'}{V})dx'$$

$$+ \int_{x_T}^{x}\int_{x_T}^{x_N} \mu_2(x,x',x'',t)\dot{v}_w(x_N,t - \frac{x_N - x''}{V})dx''dx'$$

$$\mu_1(x,x',t) = -(ff)_6 \frac{d\tilde{t}(x')}{d\alpha} (x-x') \frac{1}{V}$$

$$\dot{\mu}_1(x,x',t) = -(\dot{ff})_6 \frac{d\tilde{t}(x')}{d\alpha} (x - x') \frac{1}{V}$$

$$- (ff)_6 \frac{d\dot{\tilde{t}}(x')}{d\alpha} (x - x') \frac{1}{V}$$

$$+ (ff)_6 \frac{d\dot{\tilde{t}}(x')}{d\alpha} (x - x') \frac{\dot{V}}{V^2}$$

$$\mu_2(x,x',x'',t) = \mu_3(x,x',x'',t)\mu_4(x',x'',t)$$

$$\dot{\mu}_2(x,x',x'',t) = \mu_3\dot{\mu}_4 + \dot{\mu}_3\mu_4$$

$$\mu_3 = (ff)_6 M'(x - x') \frac{d\tilde{t}(x'')}{d\alpha} \frac{1}{V}$$

$$\dot{\mu}_3 = (\dot{ff})_6 M'(x - x') \frac{d\tilde{t}(x'')}{d\alpha} \frac{1}{V}$$

$$+ (ff)_6 \dot{M}'(x - x') \frac{d\tilde{t}(x'')}{d\alpha} \frac{1}{V}$$

$$+ (ff)_6 M'(x - x') \frac{d\dot{\tilde{t}}(x'')}{d\alpha} \frac{1}{V}$$

$$- (ff)_6 M'(x - x') \frac{d\tilde{t}(x'')}{d\alpha} \frac{\dot{V}}{V^2}$$

$$\mu_4 = \frac{(ff)_1}{I_{xx}} (x'' - x_{CG})(x' - x_{CG}) + \frac{(ff)_2}{m}$$

$$\dot{\mu}_4 = \frac{(\dot{ff})_1}{I_{xx}} (x'' - x_{CG})(x' - x_{CG}) + \frac{(\dot{ff})_2}{m}$$

$$- \frac{(ff)_1}{I_{xx}^2} (x'' - x_{CG})(x' - x_{CG})\dot{I}_{xx} - \frac{(ff)_2}{m^2} \dot{m}$$

$$- \frac{(ff)_1}{I_{xx}} (x' - x_{CG})\dot{x}_{CG} - \frac{(ff)_1}{I_{xx}} (x'' - x_{CG})\dot{x}_{CG}$$

Equations 5.11 and the expression for $\bar{g}_4(\dot{\tilde{v}}_w, x, t)$ show that impulses in $\dot{v}_w$ generate finite values of $\dot{I}_B$. Equations 5.10 and 5.11 above can now be used to replace the third and fourth rows of equations 19 of the First Quarterly Progress Report.

$$\begin{vmatrix} \beta \\ \dot{\beta} \\ I_B \\ \dot{I}_B \\ S \\ \dot{z} \\ z \end{vmatrix} = \begin{vmatrix} 1 & 0 & 0 & 0 & 0 \\ d_{21} & 0 & 0 & 0 & 0 \\ d_{31} & \bar{d}_{32} & d_{33} & d_{34} & 0 \\ \bar{d}_{41} & \bar{d}_{42} & \bar{d}_{43} & \bar{d}_{44} & 0 \\ 0 & 1 & d_{53} & d_{54} & 0 \\ 0 & 0 & 0 & 1 & 0 \\ 0 & 0 & 0 & 0 & 1 \end{vmatrix} \begin{vmatrix} \beta \\ \dot{\varphi} \\ \varphi \\ \dot{z} \\ z \end{vmatrix} + \begin{vmatrix} 0 \\ e_2 \\ 0 \\ e_4 \\ 0 \\ 0 \\ 0 \end{vmatrix} u + \begin{vmatrix} 0 \\ 0 \\ \bar{f}_3 \\ \bar{f}_4 \\ f_5 v_w \\ 0 \\ 0 \end{vmatrix} + \begin{vmatrix} 0 \\ 0 \\ 0 \\ \bar{g}_4 \\ 0 \\ 0 \\ 0 \end{vmatrix} \qquad 5.12$$

Equations 2.2 previously presented are derived from 5.12 by neglecting the time derivatives in the coefficients. It is believed the real effects of these derivatives are small and should be neglected at the present stage of the investigation.

If the wind rate has no impulses, equation 5.11 can be simplified to

$$\dot{I}_B = \bar{d}_{41}\beta + \bar{d}_{42}\dot{\varphi} + \bar{d}_{43}\varphi + \bar{d}_{44}\dot{z} + e_4 u + h_4(\tilde{v}_w, x, t) \qquad 5.13$$

where

$$h_4(\tilde{v}_w, x, t) = \bar{d}_{32}\bar{c}_1(\tilde{v}_w, t) + d_{34}\bar{c}_2(\tilde{v}_w, t)$$

$$+ \int_{x_T}^{x} \mu_5(x, x', t) v_w\left(x_N, t - \frac{x_N - x'}{V}\right) dx'$$

$$+ \int_{x_T}^{x} \int_{x_T}^{x_N} \mu_6(x, x', x'', t) v_w\left(x_N, t - \frac{x_N - x''}{V}\right) dx'' dx' \quad +$$

$$+ \mu_1\{x,x',t\}\left(\frac{V^2 + [x_N - x]\dot{V}}{V}\right)v_w\{x_N, t - \frac{x_N - x}{V}\}$$

$$- \mu_1\{x,x',t\}\left(\frac{V^2 + [x_N - x]\dot{V}}{V}\right)v_w\{x_N, t - \frac{\dot{x}_N - x_T}{V}\}$$

$$+ \mu_7\{x,t\}v_w\{x_N,t\} - \mu_8(x,t)v_w\{x_N, t - \frac{x_N - x_T}{V}\}$$

$$\mu_5\{x,x,t\} = \mu_1\{x,x',t\} - \frac{\partial}{\partial x'}\left(\left(\frac{V^2 + [x_N - x']\dot{V}}{V}\right)\mu_1(x,x',t)\right)$$

$$= \mu_1\{x,x',t\} + \frac{\dot{V}}{V}\,\mu_1(x,x',t)$$

$$+ \left(\frac{V^2 + [x_N - x']\dot{V}}{V^2}\right)(ff)_6\left[-\frac{d\tilde{t}(x')}{d\alpha}(x - x')\right.$$

$$\left. - \frac{d\tilde{t}(x')}{d\alpha}(x - x') + \frac{d\tilde{t}(x')}{d\alpha}\right]$$

$$\mu_6\{x,x',x'',t\} = \mu_2\{x,x',x'',t\} - \frac{\partial}{\partial x''}\left(\left(\frac{V^2 + [x_N - x'']\dot{V}}{V}\right)\mu_2\{x,x',x'',t\}\right.$$

$$= \mu_2\{x,x',x'',t\} + \frac{\dot{V}}{V}\,\mu_2\{x,x',x'',t\}$$

$$-\left(\frac{V^2 + [x_N - x'']\dot{V}}{V^2}\right)\left(\frac{V}{(ff)_6}\right)\mu_4\{x,x',x'',t\}\frac{\partial}{\partial x''}\mu_3\{x,x',x'',t\}$$

$$+ \frac{V}{ff_6}\,\mu_3\{x,x',x''\}\frac{\partial}{\partial x''}\mu_4\{x,x',x'',t\}$$

$$\frac{V}{ff_6}\,\frac{\partial \mu_3}{\partial x''} = M'\{x'\}(x - x')\,\frac{d\tilde{t}(x'')}{d\alpha}$$

$$+ M'\{x'\}(x - x')\,\frac{d\tilde{t}(x'')}{d\alpha}$$

$$\frac{\partial \mu_4}{\partial x''} = \frac{(ff)_1}{I_{xx}}(x' - x_{CG})$$

$$\mu_7\{x,t\} = \int_{x_T}^{x} \mu_2\{x,x',x_N,t\}dx' \frac{1}{V}$$

$$\mu_8(x,t) = \int_{x_T}^{x} \mu_2\{x,x',x_T,t\}dx'\left(\frac{V^2 + [x_N - x_T]\dot{V}}{V}\right)$$

REFERENCES

1. Anon, "Model Vehicle No. 2 for Advanced Control Studies," (77 pages, 136 figures, 1 Appendix).

2. Gilmore, Arthur et al., "Investigation of Dynamic Stability Derivatives of Vehicles Flying at Hypersonic Velocity", Air Force Flight Dynamics Laboratory Report ASD-TDR- 62-460, Sept. 1963.

3. Graham, K. D., "Minimax Control of Large Launch Boosters", Honeywell Report 12003-FTR 1 to NASA Space Flight Center on Contract NAS8-11206, 17 Sept. 1965.

4. Ashley, Holt and Zartarian, Garabed, "Piston Theory - A New Aerodynamic Tool for the Aeroelastician", Journal of the Aeronautical Sciences, Dec 1956, pp. 1109 - 1118.

5. Truxal, John G., "Control System Synthesis", McGraw-Hill, 1955.

APPENDIX B

UNCONTROLLED VEHICLE RESPONSE COVARIANCES

The response covariances of the vehicle are presented in the following five figures. They are presented for reference, and may be used to check future vehicle simulations.

APPENDIX C

RESULTS OF CONTROLLER DETERMINATION

The control feedback gains and deterministic input are presented in Figures C1.11 through C1.82.

The mean responses of the vehicle obtained with this controller are presented in Figures C2.1 through C2.7.

The response covariances produced by the controller are presented in Figures C3.1 through C3.7.

The bending-moment likelihood densities produced are presented in Figure C4.

The gimbal angle and bending moment correlation coefficients produced are presented in Figure C5.

APPENDIX D

MINIMAX RESPONSE COVARIANCES

The response covariances obtained with the minimax controller are presented in Figures D1 through D7

APPENDIX E

BENDING MOMENT RATE COEFFICIENTS

The modified bending moment rate coefficients are presented in Figures E1 and E2. The coefficient $\frac{\partial \dot{I}_b}{\partial z}$ is the negative of the coefficient $\frac{\partial \dot{I}_b}{\partial \dot{v}_w}$ presented in E1.